Nanoscale Advances

Accepted Manuscript

This article can be cited before page numbers have been issued, to do this please use: H. Cao, C. Tang, J. Duan, Z. Yang and Y. Li, *Nanoscale Adv.*, 2026, DOI: 10.1039/D6NA00092D.

ROYAL SOCIETY OF CHEMISTRY

rsc.li/nanoscale-advances

View Article Online
DOI: 10.1039/D6NA00092D

Nanoscale Advances

COMMUNICATION

Structure-Mediated Fluid-Involved Behaviors Promote Performances of Carbon-based supercapacitor

Heping Cao,[a,b]† Chengqing Tang,[a,c]† Jiashuo Duan,[a] Zhaohui Yang[b]* and Yitan Li[a, c, d]*

Received 00th January 20xx,
Accepted 00th January 20xx

DOI: 10.1039/x0xx00000x

Carbon nanotube sponges (CNTS), as promising electrode materials, were limited by inherent hydrophobicity. Herein, various TiO_2 nanostructures were synthesized inside CNTSs, providing pseudocapacitance, regulating the wettability and ion migration of the electrolyte, thereby enhancing the area-specific capacitance by up to 250%. These results offer insights for advanced energy storage systems.

Key words: carbon nanotube sponge, TiO_2 nanostructures, electrolytes, supercapacitor

Supercapacitors have attracted wide attention for their high power density[1, 2], fast charging-discharging rate with high current density[3, 4], long cyclic life[5, 6] and safety[7, 8], which are considered to be promising candidates for next-generation energy storage systems[9-12]. The performance of supercapacitors is mainly governed by the characteristics of electrode materials (specific surface area, pore structure, and conductivity), those of the electrolyte (ionic conductivity and electrochemical performance), and the compatibility between them[13, 14]. Notably, the behavior of the electrolyte within the electrode structure plays a non-negligible role[15, 16]. From a surface chemistry perspective, sufficient wetting of the electrode surface by the electrolyte is required to ensure an adequate solid-liquid contact area[17]. This is essential for forming the electric double layer[18] and facilitating electrochemical reactions[19]. Furthermore, the migration mode of ions within the electrolyte directly determines the ion transport kinetics, thereby influencing the overall performance of the supercapacitor [20, 21]. Insufficient ion migration under high-rate conditions leads to a decline in capacitive performance during rapid charge-discharge cycles[22, 23]. Therefore, developing materials possessing high porosity, large specific surface area, efficient ion transport pathways, and proper wettability with the electrolyte is of paramount importance. [14, 24, 25].

Carbon nanotube sponges (CNTS) are a class of conductive aerogels composed of multi-walled carbon nanotubes, offering multiple advantages[26-28]. The self-supporting conductive network formed by interconnected carbon nanotubes provides an exceptionally high specific surface area and abundant mesopores. These structural features facilitate electrolyte infiltration and rapid ion transport, thereby enhancing power density. Moreover, the network ensures excellent electron conduction pathways and mechanical resilience[29, 30]. However, it is important to note that pristine CNTs, when used as supercapacitor electrodes, possess inherent limitations. These include a relatively monodisperse pore structure, a singular charge storage mechanism (EDLC), and poor surface wettability (due to the highly non-polar nature of the graphitic carbon surfaces, they exhibit strong inherent hydrophobicity), all of which can restrict their charge storage capability[31, 32]. It remains a significant yet challenging task to modify the interfacial properties of CNTS without compromising their inherent structural and performance benefits[33].

Here in this study, TiO_2 nanostructures with different morphologies were introduced onto CNTs via a facile hydrothermal method, forming spherical, urchin-like, and thorn-like TiO_2@CNTs composites. Experimental and simulation results demonstrate that, compared to pristine CNTs, these TiO_2 nanostructures not only enhance electrolyte wettability but also provide additional effective solid-liquid interfaces for energy storage. The area-specific capacitance of the TiO_2@CNTS composites exhibited significant increments of

[a] National Engineering Research Center for Colloidal Materials, School of Chemistry and Chemical Engineering, Shandong University, Jinan, Shandong, 250100, P. R. China.
[b] School of Physical Science and Technology, Soochow University, Suzhou, 215006, P. R. China.
[c] Intelligent Chemical Engineering Center, Hong Kong Research Institute of Shandong University, Hong Kong SAR, P. R. China.
[d] Suzhou Research Institute, Shandong University, Suzhou, Jiangsu, 215123, P. R. China.
† These authors contributed equally to this work.
* Corresponding author. Email: yitanli@sdu.edu.cn, yangzhaohui@suda.edu.cn

View Article Online DOI: 10.1039/D6NA00092B

196.4%, 204.8%, and 250% for the spherical, urchin-like, and thorn-like TiO_2 nanostructures where thorn-like TiO_2@CNTS composites exhibit the maximal promotion in performances. This work highlights the correlation between electrolyte infiltration behavior and TiO_2 morphology, providing insights into the design of next-generation supercapacitors.

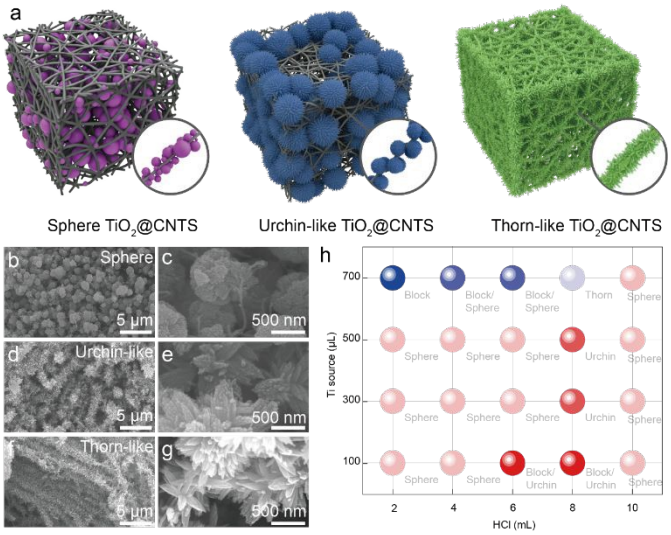

Figure 1 Morphologies of TiO_2@CNTS composites. a, Schematic illustration of TiO_2@CNTS composites. **b-c**, SEM images of spherical TiO_2@CNTS composites. **d-e**, SEM images of urchin-like TiO_2@CNTS composites. **f-g**, SEM images of thorn-like TiO_2@CNTS composites. **h**, Morphological phase diagram of TiO_2 vs. concentration.

By tuning the conditions during hydrothermal synthesis, the TiO_2 of spherical, urchin-like, and thorn-like nanostructures were synthesized on carbon nanotube sponges (CNTS) obtained by chemical vapor deposition (CVD) method.

In typical synthetic processes, the morphology of TiO_2 nanostructures evolved from spherical to urchin-like as the concentration of HCl increases from2 mL to 8 mL under low titanium precursor concentrations of 100 to 500 μ L. Conversely, TiO_2 is more likely to form bulk and thorn-likestructures under higher titanium precursor concentrations of 700 μL, while the simultaneous increases of both precursor and HCl concentrations lead to TiO_2 spheres. The morphological evolution can be ascribed to the fact that, the morphological evolution can be attributed to the carbon nanotubes serving as a self-supporting framework that provides abundant heterogeneous nucleation sites. The precursor concentration determines the initial nucleation density by controlling the supersaturation, while hydrochloric acid acts as a kinetic inhibitor, modulating the hydrolysis rate of Ti^{4+} and promoting anisotropic growth along the (001) direction through selective adsorption onto specific crystal facets. This synergistic effect between the precursor and acid concentrations leads to a structural transition from sparse spherical shapes to dense urchin-like structures, and finally to bulk-like architectures, which is consistent with previously reported growth mechanisms[34].

The hydrothermal enables the in-situ growth of TiO_2 nanostructures on carbon nanotubes. Taking spherical TiO_2@CNTS as an example, the TiO_2 particles grown directly on CNT form a "string-of-pearls" architecture, demonstrating robust interfacial bonding and sufficient contact between the nanostructures and the CNTs, indicating superior electrical conductivity and mechanical stability. Moreover, the spherical TiO_2@CNTS exhibited a contact angle of 27° (Fig. S3b) which is much lower than 98° of pristine CNTS. Urchin-like TiO_2@CNTS and thorn-like TiO_2@CNTS also exhibited excellent wettability to electrolyte, suggesting potential increase in charge storage capability of TiO_2@CNTS based supercapacitors.

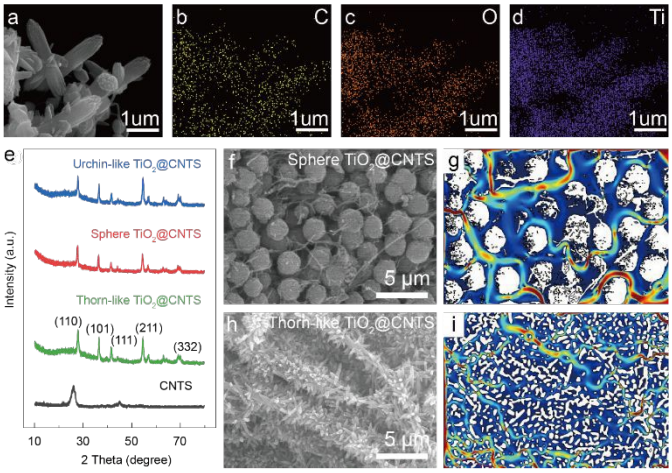

Figure 2 Characterization of TiO_2@CNTS Composites. a-d, EDS-mapping of the thorn-like TiO_2@CNTS composites. **e**, X-ray diffraction (XRD) patterns of TiO_2@CNTS composites with different morphologies. **f**, SEM image of sphere TiO_2@CNTS composites for mass transfer behavior simulation. **g**, Simulation results of mass transfer behavior in sphere TiO_2@CNTS composites. **h**, SEM image of thorn-like TiO_2@CNTS composites for mass transfer behavior simulation. **i**, Simulation results of mass transfer behavior in thorn-like TiO_2@CNTS composites.

Energy Dispersive X-ray Spectroscopy (EDS) mapping and X-ray diffraction (XRD) pattern results confirm the TiO_2@CNTS structure (Fig. 2a and b). The characteristic peaks of the hydrothermally synthesized rutile TiO_2 are clearly identified at 26.7° (110), 36.12° (101), 44.08° (111), 56.68° (211), and 69.80° (332) [35]. The characteristic peak of the CNTS appears at 26.7° , corresponding to the (002) plane of graphitic carbon. All three TiO_2 nanostructures possess a rutile crystalline phase. The resistances of TiO_2@CNTS are 0.103 K Ω /m (sphere TiO_2@CNTS composites), 0.106 K Ω /m(urchin-like TiO_2@CNTS composites), and 0.116 K Ω /m(thorn-like TiO_2@CNTS composites). The introduction of TiO_2 nanostructures not only improved the wettability but also mediate the ion flows inside

View Article Online
DOI: 10.1039/D6NA00092D

the TiO_2@CNTS composites. A laminar flow model was established in COMSOL, with the necessary hydrodynamic and physical parameters such as material type, viscosity coefficient, conductivity, and Young ‘s modulus carefully defined. It can be observed that the ion flow velocity is maximized in the central regions of the pores and decreases near the particle edges due to the fluid viscous effect. Compared to spherical and urchin-like, the thorn-like TiO_2@CNTS material possesses a more developed nanoscale pore structure, providing a greater number of transport pathways for ion adsorption and desorption near the electrode surface. Moreover, the interfacial integral length of the thorn-like TiO_2@CNTS is 1588.4 μm, which is 4 times that of the sphere TiO_2@CNTS and 2 times that of the urchin- like TiO_2@CNTS. The larger solid-liquid contact area also ensures the maximum enhancement in the capacitance performance of the Thorn-like TiO_2@CNTS sample.

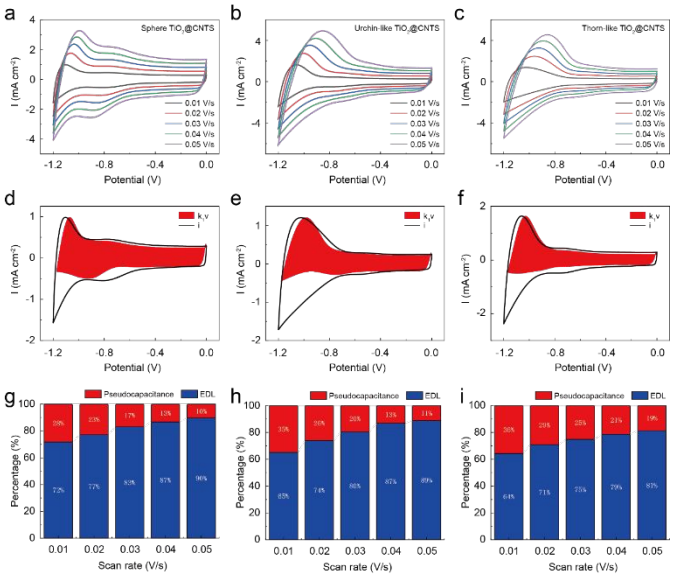

Figure 3 Capacitive performance of TiO_2@CNTS composites with various morphologies. a-c, Cyclic voltammetry (CV) curves of spherical TiO_2@CNTS composites, urchin-like TiO_2@CNTS composites and thorn-like TiO_2@CNTS composites. **d-f**, pseudo-capacitance calculation result of spherical TiO_2@CNTS composites, urchin-like TiO_2@CNTS composites and thorn-like TiO_2@CNTS composites. **g-i**, contribution value of pseudo-capacitance double layer calculation of spherical TiO_2@CNTS composites, urchin-like TiO_2@CNTS composites and thorn-like TiO_2@CNTS composites at sweep speed of 1mV/s-50mV/s.

Subsequently, we evaluated the electrochemical performance of spherical, urchin-like, and thorn-like TiO_2@CNTS composites with scan rates ranging from 10 mV/s to 50 mV/s. The thorn-like TiO_2@CNTS composites exhibit specific capacitances of 52.4 mF cm^{-2}which indicated an increasement of 57.8% and 33.3% compared to the spherical and urchin-like ones, respectively. The diffusion-controlled capacity percentages of thorn-like TiO_2@CNTS composites were 36%, 29%, 25%, 21% and 19% at 10, 20, 30, 40, and 50 mV/s while the spherical and urchin-like TiO_2@CNTS composites exhibit lower diffusion-controlled capacity percentages, indicating an increasement of pseudocapacitive contributions. Thorn-like TiO_2@CNTS composites also exhibited an increasement of up 100% in in specific capacity compared to pristine CNT.

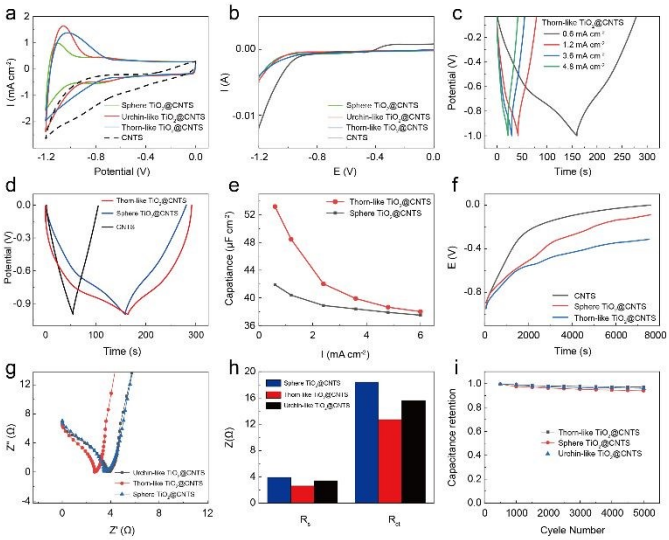

Figure 4 Comparison of charge and discharge performance of TiO_2@CNTS. a, Cyclic voltammetry (CV) curves of CNTS (black line) and spherical (green line), Urchin-like (red line) and Thorn-like (blue line) TiO_2@CNTS composites electrodes. **b**, Linear sweep voltammetry (LSV) curves of CNTS (black line) and spherical (green line), Urchin-like (red line) and Thorn-like (blue line) TiO_2@CNTS composites electrodes. **c**, Galvanostatic charge-discharge (GCD) curves of Thorn-like TiO_2@CNTS at different current densities. **d**, GCD curves of CNTS, sphere TiO_2@CNTS and Thorn-like TiO_2@CNTS at sweep speed of 0.6 mA cm^{-2}. **e**, Variation in area-specific capacitance of sphere-like TiO_2@CNTS and Thorn-like TiO_2@CNTS as a function of scan rate. **f**, Self-discharge comparison between sphere TiO_2@CNTS, Thorn-like TiO_2@CNTS and pure CNTS electrode. **g-i**, Electrochemical impedance spectroscopy (EIS, g), Equivalent Series Resistance (R_s) and Charge Transfer Resistance (R_{ct}, h) and long-term cycling stability (i) of the TiO_2@CNTS composites electrodes.

The electrochemical performance of the TiO_2@CNTS composites exhibits a significant morphology dependence (Fig. 4). The Cyclic voltammetry (CV) curves (Fig. 4a) show that the thorn-like TiO_2@CNTs possess a smaller potential difference between the reduction and oxidation peaks at a scan rate of 10 mV/s, indicating faster interfacial charge transfer kinetics and lower polarization. Linear sweep voltammetry (LSV) tests (Fig. 4b) demonstrate that the TiO_2 coating effectively suppresses electrolyte decomposition, thereby broadening the stable potential window at the electrode/electrolyte interface. Galvanostatic charge-discharge (GCD) curves (Fig. 4c-e) confirm that the spherical TiO_2@CNTS exhibit superior rate capability

(with a capacity retention of 90% at a current density of 4.8 mA cm^{-2}), and their discharge time is significantly longer than that of pristine CNTS. Furthermore, the self-discharge rate of TiO_2@CNTS is markedly reduced (Fig. 4f); due to improved wettability and optimized ion transport kinetics, its half-voltage time is extended to approximately 2500 seconds. Electrochemical impedance spectroscopy (EIS) analysis (Fig. 4g-h) reveals that the composite electrode possesses significantly lower charge transfer resistance (R_{ct}) and series resistance (R_s). Finally, the thorn-like TiO_2@CNTS maintain a capacity retention of 97% after 5000 cycles (Fig. 4i), highlighting the exceptional structural stability conferred by the enhanced integration of thorn-like TiO_2 within the three-dimensional CNTs framework.

In this study, TiO_2 nanostructures with different morphologies were successfully incorporated into carbon nanotube sponges (CNTs) using a simple hydrothermal method. Both experimental and simulation results indicate that the introduction of TiO_2 significantly enhances the hydrophilicity of the electrode and increases the effective solid–liquid contact area, thereby optimizing the fluid-involved behaviors (infiltration and ion transport) of the electrolyte. Among them, the thorn-like TiO_2@CNTs composites exhibits superior nanochannel and interfacial characteristics, demonstrating a 250% increase in area-specific capacitance compared to pristine CNTs, along with improved rate performance and cycling stability. This work reveals the intrinsic relationship between electrode nanostructure, electrolyte fluid behavior, and energy storage performance, providing clear insights for the design of next-generation high-performance supercapacitors. Furthermore, these structure-mediated design principles, specifically the transition from isotropic to anisotropic thorn-like geometries, offers a universal strategy to optimize electrolyte fluid behavior and electrochemical performance in other transition metal oxide systems such as MnO_2 and V_2O_5.

Author contributions

Heping Cao: conceptualization, methodology, hydrothermal synthesis, characterization, writing–original draft. **Chengqing Tang**: methodology, mass transfer behavior simulation, electrochemical performance evaluation, writing–original draft. **Jiashuo Duan**: data curation, chemical analysis (XRD and EDS mapping). **Zhaohui Yang**: conceptualization, supervision, validation, writing–review & editing. **Yitan Li**: conceptualization, project administration, supervision, validation, writing–review & editing.

Conflicts of interest

There are no conflicts to declare

Acknowledgement

The National Natural Science Foundation of China (grant no. 22402103), the Program of Taishan Scholar (grant no. tsqn202312040), the Natural Science Foundation of Shandong Province (grant no. 2024HWYQ-011 and 2025KJHZ014), the Natural Science Foundation of Jiangsu Province (grant no. BK20240418).

Data availability

The data supporting this article have been included as part of the supplementary information (SI). Supplementary information: SEM, FT-IR, Water Contact Angle Test, CMOSOL visualization diagram, and electrochemical performance data.

References

1. Ren, K.; Liu, Z.; Wei, T.; Fan, Z., Recent Developments of Transition Metal Compounds-Carbon Hybrid Electrodes for High Energy/Power Supercapacitors. *Nano-Micro Letters* **2021,** *13* (1), 129.
2. Ansari, S. A.; Parveen, N.; Ansari, M. Z.; Alsulaim, G. M.; Alam, M. W.; Khan, M. Y.; Umar, A.; Hussain, I.; Zhang, K., Exploring recent advances in the versatility and efficiency of carbon materials for next generation supercapacitor applications: A comprehensive review. *Progress in Materials Science* **2025,** *154*, 101493.
3. Xue, H.; Huang, P.-H.; Lai, L.-L.; Su, Y.; Strömberg, A.; Cao, G.; Fan, Y.; Khartsev, S.; Göthelid, M.; Sun, Y.-T.; Weissenrieder, J.; Gylfason, K. B.; Niklaus, F.; Li, J., High-rate metal-free MXene microsupercapacitors on paper substrates. *Carbon Energy* **2024,** *6* (5), e442.
4. Perju, A.; Zhang, D.; Wang, R. J.; Taberna, P.-L.; Gogotsi, Y.; Simon, P., Operando Tracking of Resistance, Thickness, and Mass of Ti3C2Tx MXene in Water-in-Salt Electrolyte. *Advanced Energy Materials* **2025,** *15* (20), 2405028.
5. Gao, M.; Wang, Z.; Liu, Z.; Huang, Y.; Wang, F.; Wang, M.; Yang, S.; Li, J.; Liu, J.; Qi, H.; Zhang, P.; Lu, X.; Feng, X., 2D Conjugated Metal–Organic Frameworks Embedded with Iodine for High-Performance Ammonium-Ion Hybrid Supercapacitors. *Advanced Materials* **2023,** *35* (41), 2305575.
6. Wu, D.; Zhang, Y.; Man, Z.; Zhang, H.; Zhu, X.; Ding, J.; Xu, J.; Bao, N.; Lu, W., In Situ Fabrication of Graphdiyne Nanoisland Anchored Ti3C2Tx Film to Accelerate Intercalation Pseudocapacitance Kinetics. *Advanced Energy Materials* **2024,** *14* (18), 2304404.
7. Liu, Y.; Yu, C.; Lan, S.; Liu, W.; Qiu, J., Microscopic-Level Anion & Diluent Chemistry in Electrolyte for Aqueous Supercapacitors Operating at High Voltage and Low Temperature. *Advanced Materials* **2025,** *37* (35), 2503157.
8. Dai, J.; Yang, C.; Xu, Y.; Wang, X.; Yang, S.; Li, D.; Luo, L.; Xia, L.; Li, J.; Qi, X.; Cabot, A.; Dai, L., MoS2@Polyaniline for Aqueous Ammonium-Ion Supercapacitors. *Advanced Materials* **2023,** *35* (39), 2303732.
9. Simon, P.; Gogotsi, Y.; Dunn, B., Where Do Batteries End and Supercapacitors Begin? *Science* **2014,** *343* (6176), 1210-1211.
10. Xu, T.; Li, Z.; Wang, D.; Zhang, M.; Ai, L.; Chen, Z.; Zhang, J.; Zhang, X.; Shen, L., A Fast Proton-Induced Pseudocapacitive Supercapacitor with High Energy and Power Density. *Advanced Functional Materials* **2022,** *32* (5), 2107720.
11. Arya, S.; Singh, A.; Ahmed, A.; Padha, B.; Banotra, A.; Parihar, U.; Sundramoorthy, A. K.; Dixit, S.; Vatin, N. I., Energizing tomorrow: The potential of light-driven supercapacitors in future applications. *Journal of Energy Chemistry* **2025,** *105*, 193-223.

12. Wadodkar, N. A.; Salunke, R. S.; Pawar, S. K.; Umar, A.; Ibrahim, A. A.; Akbar, S.; Ansari, S. A.; Baskoutas, S.; Shirale, D. J., Next-Generation Supercapacitors: Advances in Binder-Free Electrodes, Scalable Fabrication, and Emerging Applications. *Advanced Sustainable Systems* **2026,** *10* (1), e00599.
13. Salanne, M.; Rotenberg, B.; Naoi, K.; Kaneko, K.; Taberna, P. L.; Grey, C. P.; Dunn, B.; Simon, P., Efficient storage mechanisms for building better supercapacitors. *Nature Energy* **2016,** *1* (6), 16070.
14. Zhao, L.; Li, Y.; Yu, M.; Peng, Y.; Ran, F., Electrolyte-Wettability Issues and Challenges of Electrode Materials in Electrochemical Energy Storage, Energy Conversion, and Beyond. *Advanced Science* **2023,** *10* (17), 2300283.
15. Simon, P.; Gogotsi, Y., Perspectives for electrochemical capacitors and related devices. *Nature Materials* **2020,** *19* (11), 1151-1163.
16. Nguyen, T.; Montemor, M. d. F., Metal Oxide and Hydroxide–Based Aqueous Supercapacitors: From Charge Storage Mechanisms and Functional Electrode Engineering to Need-Tailored Devices. *Advanced Science* **2019,** *6* (9), 1801797.
17. Zhang, A.; Bi, Z.; Wang, G.; Liao, S.; Das, P.; Lin, H.; Li, M.; Yu, Y.; Feng, X.; Bao, X.; Wu, Z.-S., Regulating electrode/electrolyte interfacial chemistry enables 4.6 V ultra-stable fast charging of commercial LiCoO2. *Energy & Environmental Science* **2024,** *17* (9), 3021-3031.
18. Daraghmeh, A.; Hussain, S.; Haq, A. U.; Saadeddin, I.; Servera, L.; Ruiz, J. M., Carbon nanocomposite electrodes for electrical double layer capacitor. *Journal of Energy Storage* **2020,** *32*, 101798.
19. Olabi, A. G.; Abbas, Q.; Al Makky, A.; Abdelkareem, M. A., Supercapacitors as next generation energy storage devices: Properties and applications. *Energy* **2022,** *248*, 123617.
20. Simon, P.; Gogotsi, Y., Materials for electrochemical capacitors. *Nature Materials* **2008,** *7* (11), 845-854.
21. Islam, M. T.; Gollas, B.; Abbas, Q., Differentiating ion transport of water-in-salt electrolytes within micro- and meso-pores of a multiporous carbon electrode. *Journal of Materials Chemistry A* **2024,** *12* (37), 25504-25518.
22. Wu, Y.; Qian, Y.; Niu, B.; Chen, J.; He, X.; Yang, L.; Kong, X.-Y.; Zhao, Y.; Lin, X.; Zhou, T.; Jiang, L.; Wen, L., Surface Charge Regulated Asymmetric Ion Transport in Nanoconfined Space. *Small* **2021,** *17* (28), 2101099.
23. Augustyn, V.; Come, J.; Lowe, M. A.; Kim, J. W.; Taberna, P.-L.; Tolbert, S. H.; Abruña, H. D.; Simon, P.; Dunn, B., High-rate electrochemical energy storage through Li+ intercalation pseudocapacitance. *Nature Materials* **2013,** *12* (6), 518-522.
24. Largeot, C.; Portet, C.; Chmiola, J.; Taberna, P.-L.; Gogotsi, Y.; Simon, P., Relation between the Ion Size and Pore Size for an Electric Double-Layer Capacitor. *Journal of the American Chemical Society* **2008,** *130* (9), 2730-2731.
25. Zhang, L. L.; Zhao, X. S., Carbon-based materials as supercapacitor electrodes. *Chemical Society Reviews* **2009,** *38* (9), 2520-2531.
26. Gui, X.; Wei, J.; Wang, K.; Cao, A.; Zhu, H.; Jia, Y.; Shu, Q.; Wu, D., Carbon Nanotube Sponges. *Advanced Materials* **2010,** *22* (5), 617-621.
27. Tang, C.; Zhang, S.; Zhang, J.; Zhang, X.; Hang, Z.; Li, Y.; Yang, Z., Silicon carbide coated carbon nanotube porous sponge with super Elasticity, low Density, high thermal Resistivity, and synergistically enhanced electromagnetic interference shielding performances. *Chemical Engineering Journal* **2023,** *469*, 144011.
28. Yang, B.; Zhao, W.; Gao, Z.; Yang, J.; Shi, W.; Zhang, Y.; Su, Q.; Xu, B.; Du, G., Flexible CNT@Porous carbon sponge cathode with large mesopores for high-rate zinc-ion hybrid capacitors. *Carbon* **2024,** *218*, 118695.
29. Song, Z.; Miao, L.; Lv, Y.; Gan, L.; Liu, M., Versatile carbon superstructures for energy storage. *Journal of Materials Chemistry A* **2023,** *11* (24), 12434-12455.
30. Wadodkar, N. A.; Salunke, R. S.; Pawar, S. K.; Umar, A.; Ibrahim, A. A.; Akbar, S.; Ansari, S. A.; Baskoutas, S.; Shirale, D. J., Next-Generation Supercapacitors: Advances in Binder-Free Electrodes, Scalable Fabrication, and Emerging Applications. *Advanced Sustainable Systems n/a* (n/a), e00599.
31. Sun, J.; Li, S.; Li, Y.; Zhang, X.; Yang, Z., High-Performance Flexible Asymmetric Supercapacitor Based on Nanostructured MnO2 and Bi2O3 Decorated 3D Carbon Nanotube Sponge in an Aqueous Gel-Electrolyte. *ACS Applied Energy Materials* **2024,** *7* (17), 7450-7458.
32. Wei, Y.-M.; Kumar, K. D.; Zhang, L.; Li, J.-F., Pseudocapacitive materials for energy storage: properties, mechanisms, and applications in supercapacitors and batteries. *Frontiers in Chemistry* **2025,** *Volume 13 - 2025*.
33. Chen, L.; Tu, B.; Lu, X.; Li, F.; Jiang, L.; Antonietti, M.; Xiao, K., Unidirectional ion transport in nanoporous carbon membranes with a hierarchical pore architecture. *Nature Communications* **2021,** *12* (1), 4650.
34. Sun, B.; Shi, T.; Peng, Z.; Sheng, W.; Jiang, T.; Liao, G., Controlled fabrication of Sn/TiO2 nanorods for photoelectrochemical water splitting. *Nanoscale Research Letters* **2013,** *8* (1), 462.

View Article Online
DOI: 10.1039/D6NA00092D

Data availability

The data supporting this article have been included as part of the supplementary information (SI). Supplementary information: SEM, FT-IR, Water Contact Angle Test, CMOSOL visualization diagram, and electrochemical performance data.